Spectrum of Engineering Sciences
ISSN (e) 3007-3138 (p) 3007-312X Volume 4, Issue 3, 2026

NUMERICAL MODELING AND OPTIMIZATION OF A HIGH EFFICIENT LEAD-FREE $CsSnGeI_3$ PEROVSKITE SOLAR CELL USING SOLAR CELL CAPACITANCE SIMULATOR

Qosia Laraib[1], Azmat Ali[*2], Ahmed Salim[3], Mohsion M. Tarar[4]

[1,*2]*Department of Physics, University of Chakwal, Chakwal, Pakistan*
[3]*Department of Electrical Engineering, NAMAL University Mianwali, Pakistan*
[4]*Department of Electronics Engineering, University of Chakwal, Chakwal, Pakistan*

[1]qosialaraib@gmail.com, [*2]azmat.chakwal@gmail.com, [3]ahmed.salim@namal.edu.pk, [4]mohsin.tarar@uoc.edu.pk

DOI: http://doi.org/10.5281/zenodo.18995292

Keywords
Perovskites, Solar Energy, lead Free, SCAPS-1D, Numerical Simulations

Article History
Received: 12 January 2026
Accepted: 25 February 2026
Published: 10 March 2026

Corresponding Author: *
Azmat Ali

Abstract

In this work, a lead-free CsSnGeI3 based PSC was numerically investigated using SCAPS-1D simulator. A planar n-i-p structure using ITO/SnO2/CsSnGeI3/HTL/Au was used and the effects of various hole transport layer (CuI, P3HT and CuO) were systematically studied. SnO2 was selected as the electron transport layer because of its good band structure and high electron mobility. The thicknesses of absorber, hole transport layer and electron transport layer were optimized to have better charge transport and reduce recombination losses. The results show that performance of the device highly depends on the thickness of the absorber. Among the investigated hole transport layers, CuI and P3HT had better photovoltaic performance due to efficient hole extraction and reduced recombination but CuO showed a comparatively lower efficiency. The simulated device showed the best result in optimized condition 34.01% maximum power conversion efficiency, the open-circuit voltage of 1.13V, the short-circuit current density of 35.29 mA/cm2 and the fill factor of 84.99%. These results show the great potential of CsSnGeI3 as an environment-friendly absorber for high performance lead-free perovskite solar cells

INTRODUCTION

The increasing energy requirement at the international level, and the associated destruction of nature posed by burning fossil fuels, has forced scientists and governments to seek as an answer to these problems sustainable energy sources. Solar energy is increasingly being viewed as a potential renewable resource owing to its geographical proliferation, its capacity to scale, and its minimal environmental footprint[1]. Perovskite solar cells (PSCs) have become an area of research attention in the photovoltaic technologies because they have high-power conversion efficiencies, cost-effective processing, and excellent electronic and optical properties[2]. Perovskite solar cells were first reported in 2009 with 3.8% efficacies, and their laboratory-scale power conversion efficiencies have since risen beyond 25% to become one of the fastest-progressing photovoltaic technologies[3, 4]. Nevertheless, the traditional high-efficiency PSCs typically use lead-based halide materials, which pose severe environmental and health problems[5]. Damaged or old solar panels release lead as a potential threat to soil and ground water contamination, thus undermining the sustainability of the PSc technology[6].

In order to reduce these risks, scientists are trying to come up with lead-free alternatives which would not compromise high efficiency but offer greater environmental safety. One product of this kind is cesium tin germanium iodide ($CsSnGeI_3$), a lead free perovskite where the unhealthy lead ions have been replaced by tin ($Sn2^+$) and germanium ($Ge2^+$). This material has demonstrated suitable direct band gap, large absorption coefficients at visible wavelength and greater thermal stability that is imperative in the activity of photovoltaic [7]. In this article, potential directions to enhance the efficiency of $CsSnGeI_3$-based perovskite solar cells have been discussed by examining the parameters of the device that is conducted in the SCAPS-1D simulator[8].The performance of perovskite solar cells is analyzed in a computer with a range of different simulation packages: SILVACO ATLAS, AMPS, COMSOL and SCAPS[9]. SCAPS is particularly advantageous, that it can project devices up to seven layers in total, and even allow profiling of designs such as capacitance voltage (C-V) and capacitance frequency (C-F)[10]. SCAPS can also be used to compute several important parameters, for example spectral response, energy band alignment, AC characteristics, J-V curves and defect densities, an operator that solves equations in core semiconductor physics[11]. The ease of use and its functionality under the light and the dark also make it more useful[12]. Numerous experiments testify to the excellent correspondence of SCAPS simulations to the findings of experiments, indicating adequacy of the software in the study of photovoltaic research.[13]. SnO_2 was employed as an electron transport layer (ETL) to maximize the devices because it exhibits good conduction of electrons and because it can match its band with the $CsSnGeI_3$ absorber. CuI, CuO and P_3HT were chosen as hole transport layers because they are inclined toward unproblematic extraction of charges, recombination interference at the interface and stability of the device. They were also selected based on how compatible they were with $CsSnGeI_3$. The optimization architecture used CuI/CuO/P_3HT stack as the HTL and SnO_2 as the ETL, one that enhanced charge transport and reduced recombination losses. This setup achieved a power conversion efficiency of 34% simulated device, which highlights the potential of $CsSnGeI_3$ as a lead-free perovskite solar cell absorber in high-performance.

Materials and Method:

In the paper, the planar hetero junction perovskite solar cell was numerically modeled by considering $CsSnGeI_3$ as the lead-free absorber. The simulations have been carried out with the use of SCAPS-1D a one-dimensional tool to investigate the structure of layered solar cells. This way, the performance of the device was determined by its current voltage characteristic, band alignment, quantum efficiency, and other relevant parameters, such as open-circuit voltage (Voc), short-circuit current density (Jsc), fill factor (FF) and total power conversion efficiency (PCE). This numerical analysis rests on the fundamental equations of semiconductor. These include the Poisson and continuity relation of charge carriers (electrons and holes), which can be expressed as in equation **Error! Reference source not found.**),(**Error! Reference source not found.**) and **Error! Reference source not found.**) [14]:

$$\frac{d}{dx}\left(-\varepsilon(\mathbf{x})\frac{d\psi}{dx}\right) = q\left[p(x) - n(x) + N_D^+(x) - N_A^-(x) + p_t(x) - n_t(x)\right] \quad (1)$$

$$\frac{dp_n}{dt} = G_p - \frac{p_n - p_{n0}}{\tau_p} + p_n\mu_p\frac{d\xi}{dx} + \mu_p\xi\frac{dp_n}{dx} + D_p\frac{d^2p_n}{dx^2} \quad (2)$$

$$\frac{dn_p}{dt} = G_n - \frac{n_p - n_{p0}}{\tau_n} + n_p\mu_n\frac{d\xi}{dx} + \mu_n\xi\frac{dn_p}{dx} + D_n\frac{d^2n_p}{dx^2} \quad (3)$$

The simulated solar cell was an n-i-p based cell, and the structure was ITO/SnO_2/$CsSnGeI_3$/HTL/Au Fig. 1. Indium tin oxide was used as the transparent front contact in the structure, owing

to its high transmitted and conductivity. The back electrode was of gold (Au) selected due to its excellent work function and chemical stability that contribute to efficient hole collection. SnO_2, high mobility and well band alignment material with the absorber was used as the electron transport layer (ETL). CuI, CuO and P_3HT were individually tested as possible HTLs on the hole transport side to investigate their effect on hole extraction, recombination suppression and total device efficiency.

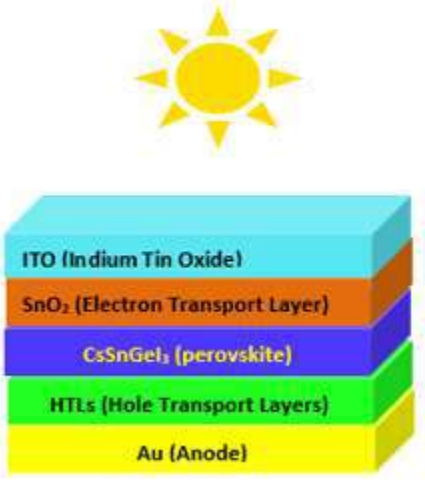

Fig. 1. Structural layout of lead-free $CsSnGeI_3$-based PSC.

Table 1. Input parameter of HTLs

Parameters	CUI [18]	P_3HT [15]	CUO [16]
Thickness (nm)	100	50	50
E_g (eV)	3.1	1.7	1.51
χ (eV)	2.1	3.5	4.07
ε_r	6.5	3.0	18.1
N_c ($1/cm^3$)	2.8×10^{19}	2.0×10^{18}	2.2×10^{19}
N_v ($1/cm^3$)	1.0×10^{19}	2.0×10^{19}	5.5×10^{20}
μ_n ($cm^2/V.s$)	1.0×10^{2}	1.8×10^{-3}	1.0×10^{2}
μ_p ($cm^2/V.s$)	4.390×10^{1}	1.8×10^{-2}	1.0×10^{-1}
N_D ($1/cm^3$)	0	0	0
N_A ($1/cm^3$)	1.0×10^{18}	1.0×10^{18}	1.0×10^{18}
N_t ($1/cm^3$)	1.0×10^{14}	1.0×10^{14}	1.0×10^{14}

Table 2. Input parameters of absorber and ETLs

Parameters	ITO [15]	SnO_2 [16]	$CsSnGeI_3$ [17]
Thickness (nm)	60	50	1.5
E_g (eV)	3.6	3.6	1.3
χ (eV)	4.1	4.0	3.9
ε_r	10	9.0	28
N_c ($1/cm^3$)	2.2×10^{18}	2.2×10^{18}	3.1×10^{18}
N_v ($1/cm^3$)	1.8×10^{19}	1.8×10^{19}	3.1×10^{18}
μ_n ($cm^2/V.s$)	5.0×10^{1}	1.0×10^{2}	9.740×10^{2}
μ_p ($cm^2/V.s$)	7.5×10^{1}	2.5×10^{1}	2.130×10^{2}
N_D ($1/cm^3$)	1.0×10^{19}	1.0×10^{18}	0
N_A ($1/cm^3$)	0	0	1.0×10^{19}
N_t ($1/cm^3$)	1.0×10^{14}	1.0×10^{14}	1.0×10^{14}

Table 1

Table 2 presents the values obtained from theoretical models, experimental findings, and reported literature. These parameters were considered while establishing the baseline configuration for initiating the simulation process. The layer thicknesses of the HTL, absorber and ETL were adjusted step by step to improve the device performance and to study how they affects the overall efficiency of the solar cell.

Results and Discussion:

Thickness Optimization of Hole Transport Layer

Hole transport layer (HTL) is an essential part of photovoltaic devices that allow selective extraction and transfer of photo generated holes from absorber to the back contact and minimizes interfacial charge recombination losses at the junction with the absorber.[19]. A thicker HTL increases the distance that holes must traverse before reaching the back contact, which can reduce recombination probability by enhancing charge carrier separation[20]. Thickness of the hole transport layer (HTL) was optimized using three materials, CuI, CuO and the P_3HT, while the absorber ($CsSnGeI_3$) and electron transport layer (ETL) remaining constant. In SCAPS-1D simulations, each HTL thickness was varied from 20nm to 200nm.**Error! Reference source not found.** demonstrates the variation of thickness on the main photovoltaic performance. To open-circuit voltage (Voc), CuI and P_3HT have almost the same value within the entire thickness range, which implies that their energy band matching with $CsSnGeI_3$ is already optimal and is not very thickness-dependent. On the contrary, CuO exhibits a slight upward trend at the decreasing thicknesses, and then, it becomes steady. As to the short-circuit current density (Jsc), CuI and P_3HT have once again shown to have constant and high values, which indicate good hole extraction and low parasitic absorption. CuO has a progressive

dependence on thickness of J_{sc}, presumably due to enhanced carrier transport. The fill factor (FF) of P_3HT and CuI does not change significantly with thickness. CuO exhibits a slight growth in FF with thickness and then it levels off. This is also the case with power conversion efficiency (PCE).

CuI and P_3HT have consistently high efficiencies throughout the thickness range, whilst CuO improve by moderate factors as a result of both V_{oc} and J_{sc} improvement. Nevertheless, its maximum efficiency is lower than of CuI and P_3HT.

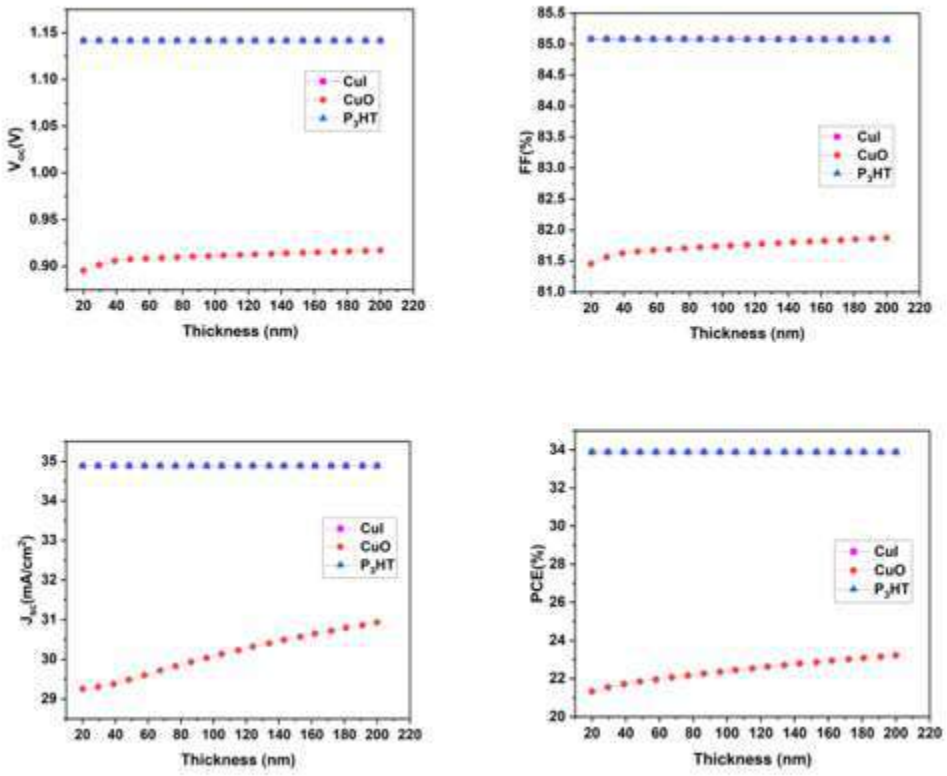

Fig. 2. Electrical parameters vs thickness of HTMs

Optimization of $CsSnGeI_3$ as the absorber layer:
The maximum performance parameters of a solar cell depend heavily on the absorber layer[21]. Photogeneration, carrier transport and recombination occur in the absorber layer that has also been described as the heart of a solar cell[22]. It has been demonstrated that the thickness and morphology of perovskite absorbers strongly effect on lifetime and diffusion length of photogenerated carriers that will in turn affects overall device performance [23, 24]. The thickness of the absorber should be well controlled to achieve maximum efficiency. When the carrier diffusion length less than the layer thickness, the probability of many carriers recombining prior contacting the electrodes is a high value that boosts series resistance and reduces efficiency. Whereas with excessively thin absorber layer, light absorption is insufficient, lower the photocurrent. Therefore, it is necessary to determine the best thickness in order to ensure the maximum efficiency of the perovskite solar cells [25, 26].
Here, the absorber layer thickness was varied from 50 nm to 2000 nm, and the calculated changes in Voc, Jsc, FF and PCE are shown in Error! R eference source not found.. For the open-circuit voltage, CuI and P_3HT also decreases slightly with increasing the absorber thickness due to the higher

recombination rate of the free charge carriers at the higher thicknesses[26]. CuO shows a slight but progressive increment in V_{oc} and this indicates improved charge extraction as the thickness go up. Both Jsc and PCE rise as absorber thickness increase, in CuI and P_3HT exhibiting a steep rise in 50 nm to 1380 nm due to the strengthening of electron-holes pair production in the absorber. Beyond this thickness the values become virtually constant since most of the incident light is already absorbed, and any additional increase in thickness primarily increases the carrier recombination rates. Of the hole transport materials (HTMs) considered, P_3HT and CuI are the most promising with the highest J_{sc} and PCE over the entire thickness. In the case of P_3HT and CuI, the FF peaks at the thinnest absorber thickness and decreases with absorber thickness because of a higher series resistance because the carriers have to traverse the longer distance through the absorber[27]. In contrast, CuO start with lower FF values compared to P_3HT and CuI, and has an initial reduction with thickness. However, at greater thicknesses, CuO exhibit a modest recovery which is due to enhanced carrier generation, that reduces the relative dominance of interface recombination losses and allows increased charge transport, resulting in modest recovery in FF while for CuI and P_3HT it stabilizes after the initial drop [28].

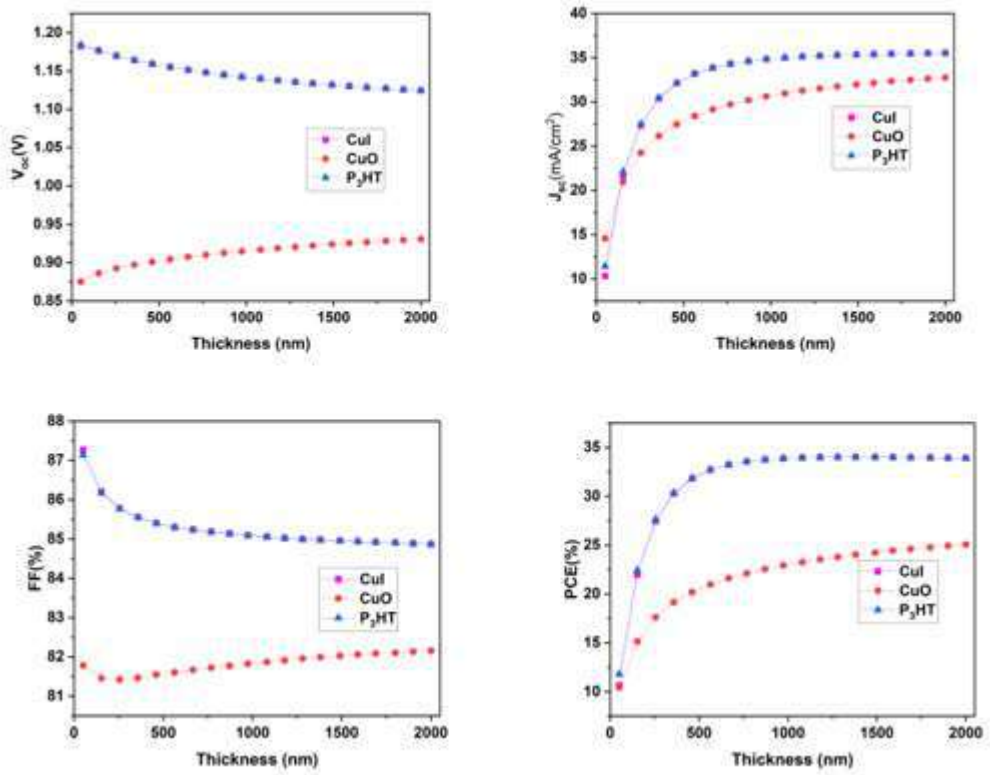

Fig. 3 .Electrical parameter vs absorber layer thickness with different ETMTable 3. Optimized thicknesses of absorber, electron and hole transport layers.

Device	ETL (nm)	Absorber (nm)	HTL (nm)
CuI	50	1380	100
P_3HT	50	1380	50
CuO	50	2000	200

Thickness Optimization of electron Transport Layer:

The electron transport layer (ETL) is an important constituent of overall device performance as it allows the optimal extraction of electrons, reduces interfacial recombination and long-term device stability[29]. Tin dioxide (SnO_2) is used as an ETL because it has good band compatibility with perovskites as well as better UV stability.[30]. Nonetheless, its thickness is of paramount importance: its thinness can cause incomplete coverage and shunting and excessive thickness can add series resistance and complicate carrier extraction[31]. Electron transport layer thickness was altered to 20 nm, and 200 nm in this simulation. Based on Error! Reference source not found., it is clear that electrical parameters remain constant when the thickness of SnO_2 is increased. The open-circuit voltage (V_{oc}) does not change significantly implying that once a continuous layer has been formed, recombination at the interface is greatly suppressed[29]. The **short-circuit current density (J_{sc})** is also steady that displays high transparency of SnO_2 and the least optical influence[32]. The thickness of the fill factor (FF) does not depend on its thickness to a large extent, which means series resistance of the ETL is insignificant [33]. These results suggest that 50nm would be suitable as a thickness of SnO_2 ETL. The film in this range provides a full coverage on the surface and allows efficient extraction of the electrons and reduction of unnecessary resistance and optical losses [34]. The thickness of 50 nm was chosen as a final configuration in this experiment to achieve maximum efficiency and stable work of the device (See **Error! Reference source not found.**).

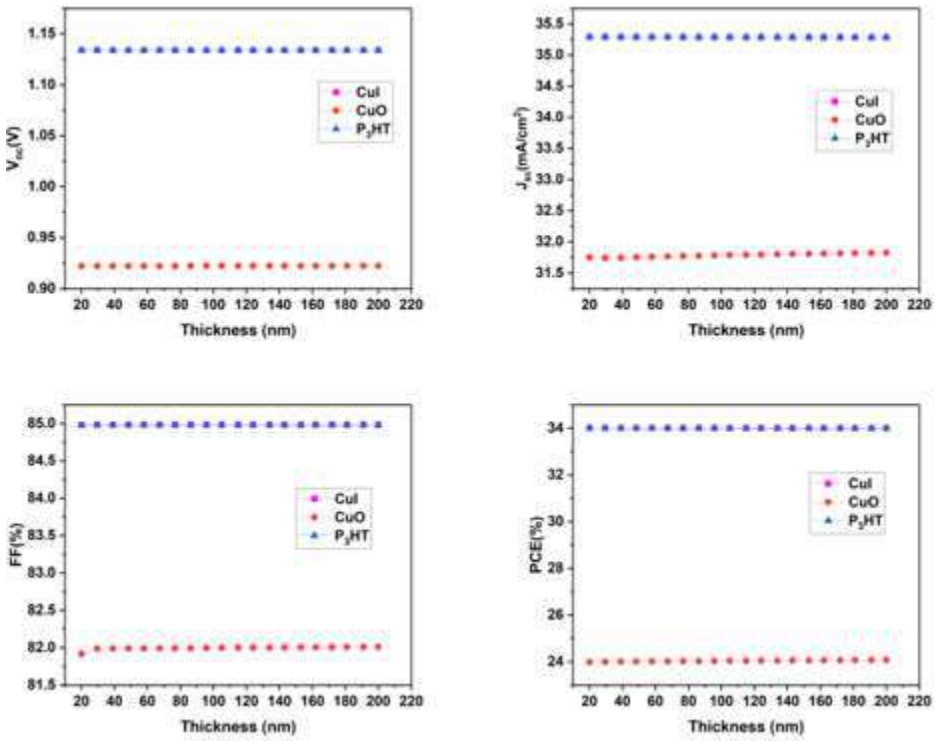

Fig. 4 . Electrical parameter vs thickness of SnO2 with different ETMs

Optimized device performance:

Energy band diagram

Fig. 5 illustrates the energy band alignment, which is useful in explaining the charge transport mechanism in the proposed solar cell. The absorber, charge transport layers, bandgap (E_g) and electron affinity (χ) are the primary components of the band diagram, along with doping concentrations and any defect states. The conduction and valence energy difference (CBO and VBO) were calculated according to the following equation to study the band alignment:

$$CBO = (\chi_{Abs} - \chi_x)$$
$$VBO = (\chi_x + E_{gx}) - (\chi_{Abs} + E_{gAbs})$$

Where χ_{Abs} and χ_x represented the electron affinities of the absorber and transport layer (HTL/ETL), while E_{gAbs} and E_{gx} denotes the corresponding band gap[35].

The CBO between the absorber and SnO_2 was found to be approximately –0.10 eV. The negative sign shows that there is a cliff structure, and this aspect may be able to promote interfacial recombination as the barrier to back-transfer of electrons is reduced. However, the size of the cliff is small which indicates that the extraction of electrons can be efficient. **Error! Reference source not found.** shows the conduction and valance band alignment values for the HTL materials. The conduction band values were 1.8 eV (CuI), 0.4 eV (P_3HT) and -0.17 eV (CuO). The CuO negative value is evidence of an adverse bending that could potentially allow an electron leakage to the HTL, leading to a lack of selectivity. Conversely, the high positive offsets of CuI and P_3HT are favorable, since they prevent electron transfer but facilitate the removal of holes [**36**]. A major detail in a hole transport is the valence band offset. The VBO values of the HTLs were determined to be 0 eV (CuI), 0 eV (P_3HT), 0.38 eV and (CuO). A positive VBO is typically a spike-type barrier, and negative VBO is a cliff structure at the interface[**37**]. Of the investigated HTLs, the materials include CuI and P_3HT which form a flat-band alignment, whereas CuO has a small positive VBO which forms a spike-like structure. Past research indicates that the optimal interface is one with a slightly negative or positive VBO, as this imparts the ability to inject holes in an efficient manner without any major obstacles[**38**].

One of the studied HTLs is CuO that create a spike (ΔE_v= +0.38 eV) whereas CuI and P_3HT have almost perfect alignment (ΔE_v= 0 eV), which ensures the efficient extraction of holes without the need of any extra barriers. It should be noted that the spike or cliff forming may not necessarily be apparent in the diagrammatic band scheme. However, by analyzing the calculated VBO values, one can clearly determine the interfacial structure. To achieve the best device performance, slightly negative or slightly positive VBO is the most appropriate, as this ensures good band alignment, and reduces recombination losses at minimal loss associated with efficient hole transport.[**38**].

Table 4. Conduction and valence band offsets for different hole transport layers (HTLs).

HTL	CBO (eV)	VBO (eV)
CuI	1.8	0
P_3HT	0.4	0
CuO	_0.17	0.38

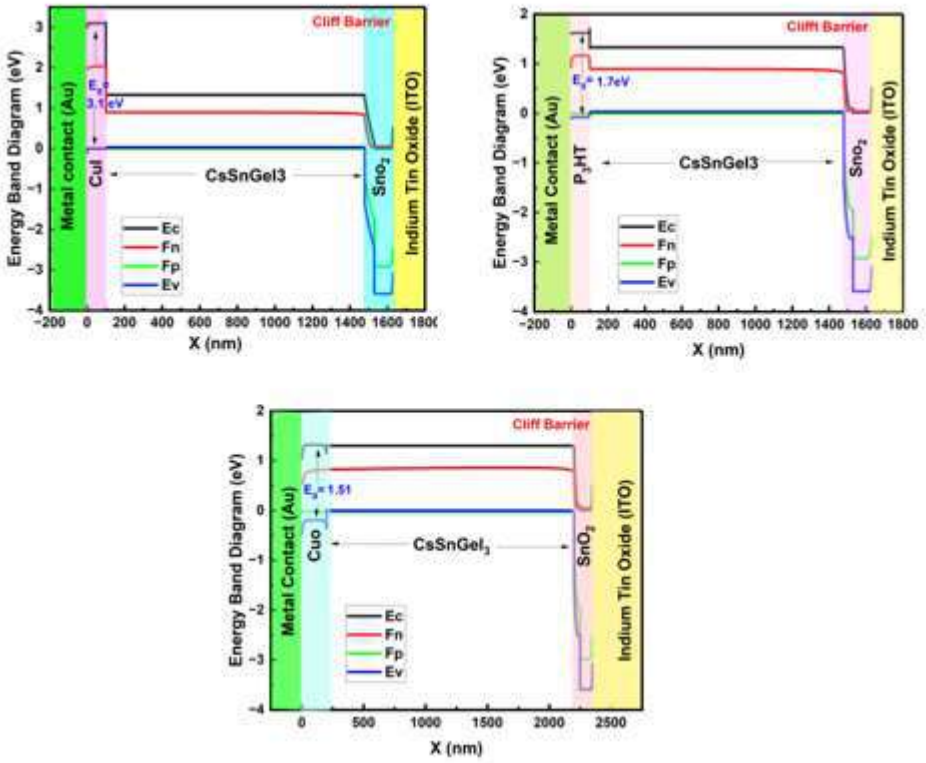

Fig. 5 .Energy band diagram of all Optimized devices with different HtLs materials

Capacitance –voltage and conductance-voltage PSc characteristics

Capacitance voltage (C-V) and conductance voltage (G-V) measurements of the devices under study were performed in the presence of light at a constant frequency of 1MHz. A higher frequency is normally selected in a way that the shallow defects and interface states are not responsive to the alternating electric field and therefore the measured capacitance is primarily one involving depletion region modulation and not traps [**39**]. The C-V and G-V characteristics are shown in a Fig. 6. In the C-V response Fig. 6 (A), the capacitive change is only slightly observable with lower forward acts but starts increasing sharper as the voltage applied approaches 0.8-1.0 V. This is because it increases photogenerated carriers thereby decreasing the depletion width and increasing storage of charge at the junction [**40**]. CuI and P3HT are the highest value of the tested materials in terms of capacitance, which means that they have a higher charge holding capacity.

The G-V characteristics Fig. 6(B) complement the C-V findings. At small forward biases, conductance remains low but increases rapidly at forward biases that exceed 0.8 V. It is worth noting that CuO has the highest conductance (0.76 $S{\cdot}cm^{-2}$ at 1.0 V) and this indicates its good ability to conduct charges when it is under illumination.

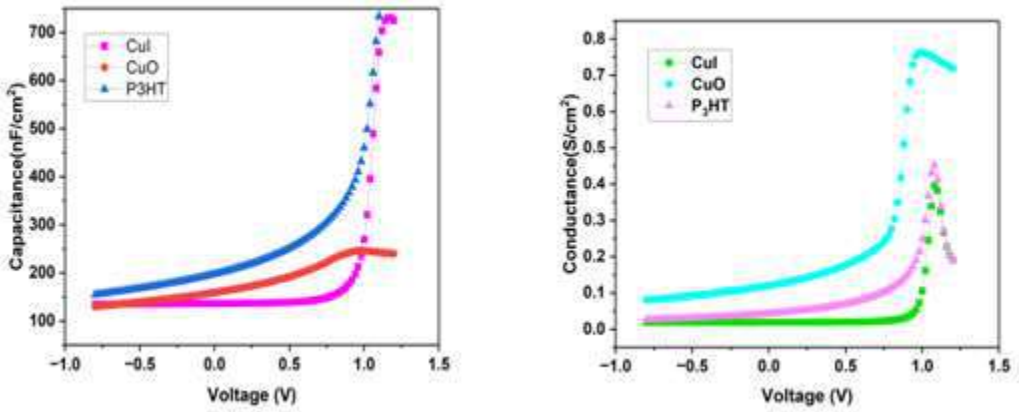

Fig. 6. (A) C-V plot for simulated PSc, (B) G-V plot for simulated PSc

J-V and QE Characteristics of optimized PSC

The performance of final device is shown in Fig. 7. J-V characteristics of perovskite solar cell were measured after optimizing HTL, ETL and absorber through three HTLs (CuO, CuI and P_3HT). The curves show that there is a difference in the current densities observed in the voltage range. This indicates that the effect of the choice of HTL on the photovoltaic properties. CuO as HTL device is characterized by the lowest performance, low current density, and low efficiency.

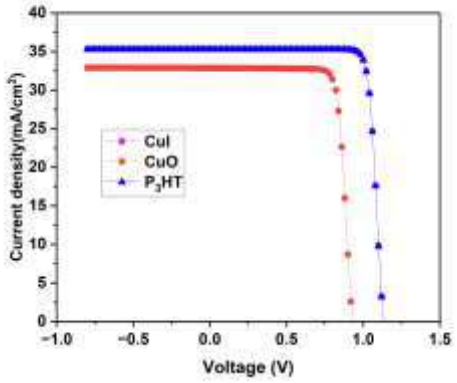

Fig. 7. J-V Characteristics of optimized PSc

This behavior originates from its relatively low hole mobility and unfavorable energy level alignment, which enhance interfacial recombination and hinder charge extraction[41]. In contrast, devices with CuI and P_3HT display significantly improved characteristics. CuI demonstrates high effectiveness due to its wide bandgap, excellent hole conductivity, and favorable alignment of its valence band with the absorber, enabling efficient charge transfer[42]. P_3HT is highest performing with regards to overall performance including stability of current density, good hole transport and recombination losses suppression[43]. **Error! Reference source not f ound.** presents the corresponding photovoltaic parameters of $\mathbf{V_{oc}}$, $\mathbf{J_{sc}}$, fill factor and efficiency. Quantum efficiency (QE) of PSC refers to the efficiency with which the device takes in photons and converts them to electrical charge. It is also described as the ratio of generated carriers to the number of photons of a specific energy absorbed by the device[44].

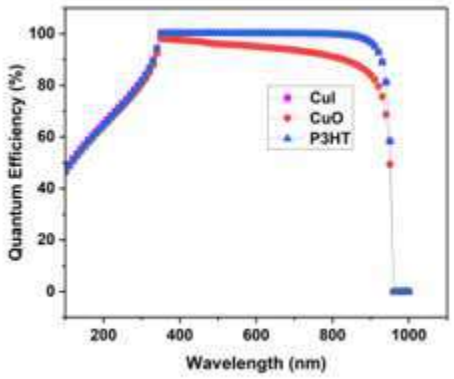

Fig. 8. Quantum efficiency of Optimized PSc

Fig 8. illustrate the efficiency of solar cell initially rises with increasing wavelength, peaks across the visible range, and then declines at longer wavelengths. For short wavelengths (< 350 nm), QE is suppressed by parasitic absorption in the ITO/SnO_2 window layers, which prevent effective carrier collection. The peak QE plateau occurs between approximately 350–750 nm, where CuI and P_3HT based device maintain nearly constant efficiencies above 95%, while CuO device maintain good response but show earlier decline and CuO device show less QE. Beyond 830 nm, QE drops to zero, as photons no longer have sufficient energy to generate carriers.

Conclusion

In this study, a lead-free perovskite solar cell was analyzed in more detail through numerical simulations of SCAPS-1D. An ITO/SnO_2/absorber/HTLs/Au literature planar layout was investigated to analyze and optimize photovoltaic performance. The optimization was done in stages starting with hole transport layer (HTL) then absorber thickness and lastly electron transport layer (ETL).The recombination and carrier generation is shown to be strictly controlled by the absorber thickness. The thickness beyond which no more benefits of light-absorption were to be obtained was optimal, due to recombination losses. Furthermore, the choice of HTL had a significant influence on behavior of the devices. Among the candidates, the performance of CuO was the lowest due to the absence of mobility and similar energy level responsiveness, but P_3HT and CuI exhibited good performance with nearly equal efficiencies about 34% with regard to good band alignment, excellence of hole transport, and minimal recombination losses.

Overall, this research shows that the efficiency of power conversion in perovskite solar cells is greatly enhanced when the absorber, HTL, and ETL layers are optimized. The findings that we have achieved can offer a potential path to the manufacturing of cost-effective high-performing and stable lead-free perovskite devices.

Table 5. Device performance after optimization parameters.

Devices	V_{oc}(V)	J_{sc}(mA/cm^2)	FF(%)	PCE(%)
ITO/SnO_2/$CsSnGeI_3$/CUI/Au	1.13	35.29	84.99	34.01
ITO/SnO_2/$CsSnGeI_3$/P_3HT/Au	1.13	35.28	84.98	34.00
ITO/SnO_2/$CsSnGeI_3$/CUO/Au	0.93	32.85	82.17	25.15

References

1. Kalair, A., et al., *Role of energy storage systems in energy transition from fossil fuels to renewables.* Energy Storage, 2021. **3**(1): p. e135. **https://doi.org/10.1002/est2.135**
2. Jena, A.K., A. Kulkarni, and T. Miyasaka, *Halide perovskite photovoltaics: background, status, and future prospects.* Chemical reviews, 2019. **119**(5): p. 3036-3103.**https://doi.org/10.1021/acs.chemrev.8b00539**
3. Kojima, A., et al., *Organometal halide perovskites as visible-light sensitizers for photovoltaic cells.* Journal of the american chemical society, 2009. **131**(17): p. 6050-6051.**https://doi.org/10.1021/ja809598r**
4. Kim, J.Y., et al., *High-efficiency perovskite solar cells.* Chemical reviews, 2020. **120**(15): p. 7867-7918.**https://doi.org/10.1021/acs.chemrev.0c00107**
5. Raoui, Y., et al., *Harnessing the potential of lead-free Sn–Ge based perovskite solar cells by unlocking the recombination channels.* Sustainable Energy & Fuels, 2021. **5**(18): p. 4661-4667.**https://doi.org/10.1039/D1SE00687H**
6. Bi, H., et al., *Multistrategy preparation of efficient and stable environment-friendly lead-based perovskite solar cells.* ACS Applied Materials & Interfaces, 2022. **14**(31): p. 35513-35521.**https://doi.org/10.1021/acsami.2c06032**
7. Azizman, M.S.A., et al., *Mixed cations tin-germanium perovskite: A promising approach for enhanced solar cell applications.* Heliyon, 2024. **10**(8).**https://doi.org/10.1016/j.heliyon.2024.e29676**
8. Abdulmalik, M.O., et al., *Numerical study of 25.459% alloyed inorganic lead-free perovskite CsSnGeI3-based solar cell by device simulation.* East European Journal of Physics, 2022(4): p. 125-135.**https://doi.org/10.26565/2312-4334-2022-4-12**
9. Salgado-Conrado, L., C. Álvarez-Macías, and B. Reyes-Durán, *A review of simulation tools for thin-film solar cells.* Materials, 2024. **17**(21): p. 5213.**https://doi.org/10.3390/ma17215213**
10. Katunge, E.K., G.G. Njema, and J.K. Kibet, *Theoretical analysis of the electrical characteristics of lead-free formamidinium tin iodide solar cell.* IET Optoelectronics, 2023. **17**(5): p. 220-236. **https://doi.org/10.1049/ote2.12104**
11. Hosseini, S.R., et al., *Investigating the effect of non-ideal conditions on the performance of a planar CH3NH3PbI3-based perovskite solar cell through SCAPS-1D simulation.* Heliyon, 2022. **8**(11).**https://doi.org/10.1016/j.heliyon.2022.e11471**
12. Mushtaq, S., et al., *Performance optimization of lead-free MASnBr3 based perovskite solar cells by SCAPS-1D device simulation.* Solar Energy, 2023. **249**: p. 401-413.**https://doi.org/10.1016/j.solener.2022.11.050**
13. Gholami-Milani, A., et al., *Performance analyses of highly efficient inverted all-perovskite bilayer solar cell.* Scientific Reports, 2023. **13**(1): p. 8274.**https://doi.org/10.1038/s41598-023-35504-x**

14. Rahman, M.B., et al., *Selection of a compatible electron transport layer and hole transport layer for the mixed perovskite FA 0.85 Cs 0.15 Pb (I 0.85 Br 0.15) 3, towards achieving novel structure and high-efficiency perovskite solar cells: a detailed numerical study by SCAPS-1D.* RSC advances, 2023. **13**(25): p. 17130-17142.**https://doi.org/10.1039/D3RA02170J**
15. Banik, S., et al., *Numerical simulation and performance optimization of a lead-free inorganic perovskite solar cell using SCAPS-1D.* Heliyon, 2024. **10**(1).**https://doi.org/10.1016/j.heliyon.2024.e23985**
16. Talukder, M.J., *A comprehensive investigation involving numerous HTL and ETL layers to design and simulate high-efficiency Ca 3 AsI 3-based perovskite solar cells.* Available at SSRN 5075253, 2024.**https://doi.org/10.1016/j.inoche.2024.113647**
17. Hossain, M.M., et al., *Computation and analysis of highly stable and efficient non-toxic perovskite CsSnGeI3 based solar cells to enhance efficiency using SCAPS-1D software.* Signal and Image Processing Letters, 2023. **5**(2): p. 9-19.**https://doi.org/10.31763/simple.v5i2.66**
18. Hossain, M.K., et al., *Effect of various electron and hole transport layers on the performance of CsPbI3-based perovskite solar cells: a numerical investigation in DFT, SCAPS-1D, and wxAMPS frameworks.* ACS omega, 2022. **7**(47): p. 43210-43230.**https://doi.org/10.1021/acsomega.2c05912**
19. Stolterfoht, M., et al., *The impact of energy alignment and interfacial recombination on the internal and external open-circuit voltage of perovskite solar cells.* Energy & environmental science, 2019. **12**(9): p. 2778-2788.**https://doi.org/10.1039/C9EE02020A**
20. Hossain, M.K., et al., *An investigation of hole transport layers and electron transport layers to produce highly efficient K2TiI6-based perovskite solar cells.* Scientific Reports, 2025. **15**(1): p. 19014.**https://doi.org/10.1038/s41598-025-98351-y**
21. Hosen, A. and S.R. Al Ahmed, *Performance analysis of SnS solar cell with a hole transport layer based on experimentally extracted device parameters.* Journal of Alloys and Compounds, 2022. **909**: p. 164823.**https://doi.org/10.1016/j.jallcom.2022.164823**
22. Burschka, J., et al., *Sequential deposition as a route to high-performance perovskite-sensitized solar cells.* Nature, 2013. **499**(7458): p. 316-319.**https://doi.org/10.1038/nature12340**
23. Valeti, N.J., K. Prakash, and M.K. Singha, *Numerical simulation and optimization of lead free CH3NH3SnI3 perovskite solar cell with CuSbS2 as HTL using SCAPS 1D.* Results in Optics, 2023. **12**: p. 100440.**https://doi.org/10.1016/j.rio.2023.100440**
24. Guo, Y., et al., *Effects of transition metal substituents on interfacial and electronic structure of CH3NH3PbI3/TiO2 interface: a first-principles comparative study.* Nanomaterials, 2019. **9**(7): p. 966.**https://doi.org/10.3390/nano9070966**
25. Lazemi, M., S. Asgharizadeh, and S. Bellucci, *A computational approach to interface engineering of lead-free CH 3 NH 3 SnI 3 highly-efficient perovskite solar cells.* Physical Chemistry Chemical Physics, 2018. **20**(40): p. 25683-25692.**https://doi.org/10.1039/C8CP03660H**
26. Liu, M., M.B. Johnston, and H.J. Snaith, *Efficient planar heterojunction perovskite solar cells by vapour deposition.* Nature, 2013. **501**(7467): p. 395-398.**https://doi.org/10.1038/nature12509**

27. Abdelaziz, S., et al., *Investigating the performance of formamidinium tin-based perovskite solar cell by SCAPS device simulation.* Optical materials, 2020. **101**: p. 109738.**https://doi.org/10.1016/j.optmat.2020.109738**
28. Kumar, M., et al., *An optimized lead-free formamidinium Sn-based perovskite solar cell design for high power conversion efficiency by SCAPS simulation.* Optical Materials, 2020. **108**: p. 110213.**https://doi.org/10.1016/j.optmat.2020.110213**
29. Stolterfoht, M., et al., *Visualization and suppression of interfacial recombination for high-efficiency large-area pin perovskite solar cells.* Nature Energy, 2018. **3**(10): p. 847-854.**https://doi.org/10.1038/s41560-018-0219-8**
30. Zanoni, K.P., et al., *Tin (IV) oxide electron transport layer via industrial-scale pulsed laser deposition for planar perovskite solar cells.* ACS Applied Materials & Interfaces, 2023. **15**(27): p. 32621-32628.**https://doi.org/10.1021/acsami.3c04387**
31. Hoang Huy, V.P. and C.-W. Bark, *Review on surface modification of SnO2 electron transport layer for high-efficiency perovskite solar cells.* Applied Sciences, 2023. **13**(19): p. 10715.**https://doi.org/10.3390/app131910715**
32. Uddin, A. and H. Yi, *Progress and challenges of SnO2 electron transport layer for perovskite solar cells: A critical review.* Solar RRL, 2022. **6**(6): p. 2100983.**https://doi.org/10.1002/solr.202100983**
33. Suh, W.S., et al., *Optimal film thickness and Sn oxidation state of sputter-deposited SnO 2 electron transport layers for efficient perovskite solar cells.* Sustainable Energy & Fuels, 2024. **8**(22): p. 5214-5224.**https://doi.org/10.1039/D4SE00911H**
34. Kam, M., et al., *Room-temperature sputtered SnO2 as robust electron transport layer for air-stable and efficient perovskite solar cells on rigid and flexible substrates.* Scientific reports, 2019. **9**(1): p. 6963.**https://doi.org/10.1038/s41598-019-42962-9**
35. Noman, M., Z. Khan, and S.T. Jan, *A comprehensive review on the advancements and challenges in perovskite solar cell technology.* RSC advances, 2024. **14**(8): p. 5085-5131.**https://doi.org/10.1039/D3RA07518D**
36. Shah, B.S., et al., *SCAPS 1D based study of hole and electron transfer layers to improve MoS2–ZrS2 solar cell efficiency.* Modelling and Simulation in Materials Science and Engineering, 2024. **32**(6): p. 065015.**https://doi.org/10.1088/1361-651X/ad5a2b**.
37. Dar, S.A., B. Want, and B.S. Sengar, *Enhancing efficiency: A study on all-inorganic CsSnBr3 metal halide perovskites with micro-band offset using DFT and SCAPS-1D modeling.* Solar Energy, 2024. **284**: p. 113051.**https://doi.org/10.1016/j.solener.2024.113051**
38. Barthwal, S., et al., *Band offset engineering in antimony sulfide (Sb2S3) solar cells, using SCAPS simulation: A route toward PCE> 10%.* Optik, 2023. **282**: p. 170868.**https://doi.org/10.1016/j.ijleo.2023.170868**
39. Dharmadasa, I., et al., *Perovskite solar cells: a deep analysis using current–voltage and capacitance–voltage techniques.* Journal of materials science: Materials in electronics, 2019. **30**(2): p. 1227-1235.**https://doi.org/10.1007/s10854-018-0390-5**

40. Roy, P. and A. Khare, *Understanding the strategies to attain the best performance of all inorganic lead-free perovskite solar cells: Theoretical insights.* International Journal of Energy Research, 2022. **46**(11): p. 15881-15899.**https://doi.org/10.1002/er.8287**
41. Haddad, J., et al., *Analyzing interface recombination in lead-halide perovskite solar cells with organic and inorganic hole-transport layers.* Advanced materials interfaces, 2020. **7**(16): p. 2000366.**https://doi.org/10.1002/admi.202000366**
42. Sun, W., et al., *Room-temperature and solution-processed copper iodide as the hole transport layer for inverted planar perovskite solar cells.* Nanoscale, 2016. **8**(35): p. 15954-15960.**https://doi.org/10.1039/C6NR04288K**
43. Zhou, P., et al., *Efficient and stable mixed perovskite solar cells using P3HT as a hole transporting layer.* Journal of Materials Chemistry C, 2018. **6**(21): p. 5733-5737.**https://doi.org/10.1039/C8TC01345D**
44. Chakraborty, K., M.G. Choudhury, and S. Paul, *Numerical study of Cs2TiX6 (X= Br−, I−, F− and Cl−) based perovskite solar cell using SCAPS-1D device simulation.* Solar Energy, 2019. **194**: p. 886-892.**https://doi.org/10.1016/j.solener.2019.11.005**